

# DWTNeRF: Boosting Few-shot Neural Radiance Fields via Discrete Wavelet Transform

Hung Nguyen    Runfa Blark Li    Truong Nguyen  
 Video Processing Lab, UC San Diego  
 {hun004, runfa, tqn001}@ucsd.edu

## Abstract

Neural Radiance Fields (NeRF) has achieved superior performance in novel view synthesis and 3D scene representation, but its practical applications are hindered by slow convergence and reliance on dense training views. To this end, we present DWTNeRF, a unified framework based on Instant-NGP’s fast-training hash encoding. It is coupled with regularization terms designed for few-shot NeRF, which operates on sparse training views. Our DWTNeRF includes a novel Discrete Wavelet loss that allows explicit prioritization of low frequencies directly in the training objective, reducing few-shot NeRF’s overfitting on high frequencies in earlier training stages. We additionally introduce a model-based approach, based on multi-head attention, that is compatible with INGP-based models, which are sensitive to architectural changes. On the 3-shot LLFF benchmark, DWTNeRF outperforms Vanilla NeRF by 15.07% in PSNR, 24.45% in SSIM and 36.30% in LPIPS. Our approach encourages a re-thinking of current few-shot approaches for INGP-based models.

## 1. Introduction

NeRF [21] have emerged as a powerful method for reconstructing 3D scenes from a set of 2D images. This can generate photorealistic views from novel angles. Its properties have enabled applications in medical imaging [4, 5], robotics [44, 45], virtual reality [36, 38], autonomous driving [19, 32], and many more.

However, a disadvantage of NeRF is its slow convergence, which can take several hours to render a scene [28]. Besides, it requires a dense set of training views [29]. Those problems can hinder NeRF’s practical uses. For the former problem, INGP [22] introduced a multi-resolution hash encoding that dramatically reduces training time. However, to the best of our knowledge, limited research has been conducted on few-shot INGP-based NeRF. Therefore, our work will focus on addressing this gap.

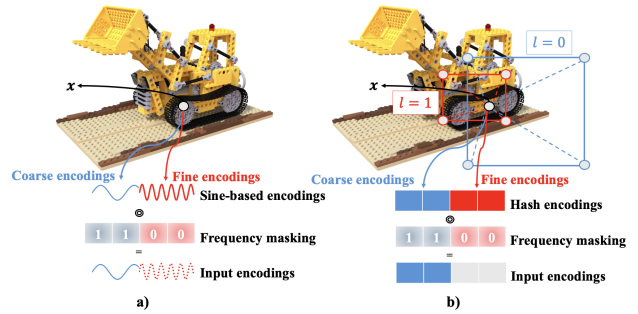


Figure 1. Comparison of frequency masking as applied to sine-based encoding (a) and multi-resolution hash encoding (b). To be compatible with frequency masking [39], the later portions of the encoded inputs  $\gamma(\mathbf{x})$  must strictly correspond to high frequencies. For the hash encoding, those input portions correspond to fine resolutions, which are not interchangeable with high frequencies.

INGP has distinct characteristics that make some recent few-shot approaches incompatible. Firstly, its positional encoding is based on multi-resolution. This differs from the sine-based encoding [26] in Vanilla NeRF and similar works, which *explicitly* map inputs to high frequencies for learning intricate details. The sine-based encoding supports frequency masking [39], a regularization strategy that element-wise masks high-frequency inputs early in training to prevent overfitting. However, applying this to INGP, as in Figure 1, assumes fine resolutions correspond to high frequencies, which is not strictly true. For instance, a point on a flat, monochromatic surface remains low frequency, irrespective of resolution. We will show in Section 5.4 that rendering improvements can be achieved just by removing frequency masking from an INGP-based NeRF.

Secondly, INGP is fast-converging. Its aggressive optimization dynamics amplify the impact of even small adjustments. This is a challenge for model-based methods, which focus on tweaking the Vanilla MLP’s architecture in NeRF to improve its few-shot capabilities [46]. We will again show

in Section 5.4 that slight architectural changes, like simply adding *one* more layer and some residual connections, degrade few-shot INGP’s performance.

The above discussion yields a two-fold motivation. Firstly, given the proven effectiveness of frequency-based regularization, we need to devise a method that accomplishes the same idea, but compatible with INGP. To this end, we decompose the rendered and ground-truth scenes into levels of frequencies, using the Discrete Wavelet Transform. Their frequency-space differences are minimized by our novel Discrete Wavelet loss. By setting a higher weight to low-frequency discrepancies, we can *explicitly* prioritize their learning right in the training objective. Secondly, given the proven effectiveness of model-based methods, we need to devise a method that does not degrade INGP, which is sensitive to architectural changes. Our focus is on modelling the color-density interactions. While better modelled with separate MLP branches, they still require some levels of interactions [46]. We call this the “cross-branch interactions”. To this end, we propose using multi-head attention modules at the input and output levels. This does not incur architectural changes to the MLP, and does not degrade performance like other model-based methods.

In summary, our contributions are as follows:

- A unified framework, DWTNeRF, that blends the following prevalent approaches towards few-shot INGP-based NeRF:
- *Regularization-based* approach with a novel Discrete Wavelet loss that explicitly decomposes the scenes into low and high-frequencies, enabling prioritizing low frequencies at earlier training stages;
- *Model-based* approach to enable cross-branch interactions using multi-head attention, which is compatible with fast-converging INGP;
- Through comprehensive experiments, we demonstrate that the proposed DWTNeRF is highly competitive with state-of-the-art methods, especially under highly challenging 2- to 4-shot conditions. The proposed DWTNeRF is also much faster due to being INGP-based.

## 2. Related Works

### 2.1. Neural Radiance Fields

NeRF [21] has attained wide popularity in novel view synthesis and 3D scene representation tasks. It is self-supervised, able to construct 3D scenes without any 3D ground-truth data, relying only on multi-view images. Compared to earlier view synthesis methods, it is highly photorealistic. However, Vanilla NeRF is limited in practical applications [7]. Therefore, further research has been aimed at faster training & rendering [41], generalizability [40], dynamic scenes [25], 3D generation [12], etc. In the sub-field of fast-training NeRF, INGP [22] introduced a multi-resolution hash encod-

ing whose CUDA implementation can render scenes within seconds. On top of INGP, we focus on another sub-field: few-shot NeRF, which aims to reduce its high dependence on a dense training set of multi-view images.

### 2.2. Few-shot NeRF

**Prior-based methods** Those enable few-shot NeRF by training a generalized model on a large dataset of diverse scenes or by incorporating pre-trained priors in their training objectives. pixelNeRF [42] leveraged a feature encoder to extract image features from sparse input views, and conditioned a NeRF on these features. DietNeRF [11] introduced a semantic consistency loss that minimizes discrepancies in embeddings of rendered and ground-truth views, encouraging high-level semantic similarities. RegNeRF [23] leveraged a trained normalizing flow model to regularize color patches of unobserved views. SparseNeRF [8] introduced a local depth ranking loss based on priors from a trained depth estimation model. SPARF [33] minimized coordinate-space discrepancies between pixel matches in multiple ground-truth views, predicted by a trained feature matching model. This encourages a global and geometrically accurate solution. GeCoNeRF [17] extended this concept of geometric consistency to the feature-space, regularizing both semantically and structurally.

**Regularization-based methods** Those enable few-shot NeRF by additionally introducing regularization terms, optimizing in a per-scene manner. InfoNeRF [16] introduced a KL-divergence loss that enforces consistent density distributions across neighboring rays. RegNeRF [23] introduced a depth smoothness loss that penalizes depth discrepancies between neighboring points. Mip-NeRF 360 [1] introduced a distortion loss that reduces floating artifacts by minimizing the weighted distances between sampled points. DiffusionNeRF [37] introduced a full geometry loss that encourages the weights of sampled points along each ray to sum to unity, which ensures the rays are absorbed fully by the scene’s geometry. Another significant work is FreeNeRF [39], which did not introduce new terms but proposed masking input encodings in a coarse-to-fine manner, preventing NeRF from overfitting on high frequencies in early training stages. CombiNeRF [2], which our work is based on, synergistically combined all these techniques on top of INGP, achieving SOTA results.

**Model-based methods** [46] shows that Vanilla MLP is not sufficient for few-shot NeRF. They introduced two main modules, which we term “Residual Connections” and “Element-wise Cross-branch Interactions”. In the former, the encoded inputs are fed into each MLP layer, ensuring a shorter connection between the inputs and outputs. This is similar to ResNet [9] & DenseNet’s [10] residual connections. In the latter, the colors & densities are modeled using separate MLP branches, and cross-branch interactions

are learned by a simple element-wise addition between corresponding layers. This pioneering work presented a new direction towards few-shot NeRF: adjusting Vanilla MLP’s architecture.

However, aside from DiffusioNeRF and CombiNeRF, none of the works above are based on INGP. Our experiments reveal that not all few-shot methods are transferable across Vanilla NeRF and INGP. Precisely, frequency regularization and model-based approaches are not trivially transferable. This is due to INGP’s multi-resolution encoding and fast convergence, as explained in Section 1. To this end, we present a blend of regularization- and model-based approaches that are INGP-compatible.

### 3. Preliminaries

#### 3.1. Neural Radiance Fields

The key idea of NeRF is to optimize a 5D plenoptic function that represents a 3D volume,  $f(\mathbf{x}, \mathbf{d})$ , where  $\mathbf{x} = (x, y, z)$  is a 3D spatial position viewed from a unit direction  $\mathbf{d} = (\theta, \phi)$ .  $f$  outputs a view-dependent RGB color  $\mathbf{c}$  and a differential volume density  $\sigma$ , and is parameterized by an MLP. To calculate the colors in a pixel grid, we start by shooting a ray  $\mathbf{r}(t)$  into the 3D scene, through a pixel  $\mathbf{p}$ . The ray has an origin at  $\mathbf{o}$  and a 3D direction  $\mathbf{d}$ . Along the ray, we sample multiple points.  $f$  learns the color  $\mathbf{c}$  and the density  $\sigma$  of each point. The final color of the pixel  $\mathbf{p}$ ,  $\mathbf{c}(\mathbf{r})$ , is calculated with simplified volume rendering [13]:

$$\mathbf{c}(\mathbf{r}) = \int_{t_n}^{t_f} T(t) \sigma(\mathbf{r}(t)) \mathbf{c}(\mathbf{r}(t), \mathbf{d}) dt \quad (1)$$

where  $t_n$  and  $t_f$  denote the lower and higher-bound spatial positions of the sampled points. The color of a point  $t$  is  $\mathbf{c}(\mathbf{r}(t), \mathbf{d})$ , weighted by the point’s density  $\sigma(\mathbf{r}(t))$ . This is again weighted by the transmittance  $T(t)$ :

$$T(t) = \exp\left(-\int_{t_n}^t \sigma(\mathbf{r}(s)) ds\right)$$

which can be interpreted as the probability that the ray traverses uninterrupted from  $t_n$  to  $t$  [24]. The process repeats for all rays forming a batch  $\mathcal{R}$ . NeRF is optimized by minimizing the MSE between predicted colors  $\mathbf{c}(\mathbf{r})$  and ground-truth colors  $\mathbf{c}_{gt}(\mathbf{r})$ , under the same pose  $\mathbf{p}$ :

$$\mathcal{L}_{MSE} = \frac{1}{|\mathcal{R}|} \sum_{\mathbf{r} \in \mathcal{R}} \|\mathbf{c}(\mathbf{r}) - \mathbf{c}_{gt}(\mathbf{r})\|_2^2$$

#### 3.2. Discrete Wavelet Transform (DWT)

Here, we explain the DWT, which our Discrete Wavelet loss (Section 4.2) is based on. Suppose that the ray batch  $\mathcal{R}$  consists of adjacently sampled rays  $\mathbf{r}$ . This amounts to a 2D image  $\mathbf{I}$ , which can be compared with the ground-truth

image  $\mathbf{I}_{gt}$ . We can perform the DWT on  $\mathbf{I}$  to receive the four following sub-bands:

$$\begin{aligned} \mathbf{I}^{LL} &= \mathbf{LIL}^T; \mathbf{I}^{LH} = \mathbf{HIL}^T \\ \mathbf{I}^{HL} &= \mathbf{LIH}^T; \mathbf{I}^{HH} = \mathbf{HIH}^T \end{aligned}$$

where  $\mathbf{L}$  and  $\mathbf{H}$  are the low-pass and high-pass 2D matrices, respectively.  $\mathbf{L}$  is constructed as:

$$\mathbf{L} = \begin{pmatrix} \dots & \dots & \dots & & & & & & \\ \dots & \ell_{-1} & \ell_0 & \ell_1 & \dots & & & & \\ & & \dots & \ell_{-1} & \ell_0 & \ell_1 & \dots & & \\ & & & & & & \dots & \dots & \end{pmatrix}$$

where  $\ell_k$  is the  $k$ -indexed coefficient of the 1D low-pass wavelet filter  $\ell$ . If  $\ell$  is orthogonal, then the 1D high-pass filter  $h$  is derived trivially from  $\ell$ , and  $\mathbf{H}$  trivially from  $\mathbf{L}$  [30].  $\mathbf{I}^{LL}$  is called the LL sub-band of  $\mathbf{I}$ , and so on for other components. Intuitively,  $\mathbf{I}^{LL}$  represents the low-frequency components of the image.  $\mathbf{I}^{LH}$  and  $\mathbf{I}^{HL}$  represent high frequencies in one direction, but low frequencies in another. Finally,  $\mathbf{I}^{HH}$  represents the high frequencies in both vertical & horizontal directions. Note that each row of  $\mathbf{L}$  is just a delayed version of the same 1D filter  $\ell$ . From row to row,  $\ell$  skips every other elements. The same goes for  $\mathbf{H}$ . This means that, in terms of size, the sub-bands are only a quarter of the original image. This is a concern in applying the DW loss, which we will explain later.

## 4. Methodology

### 4.1. Overview

Figure 2 shows the architecture diagram of our DWTNeRF. It consists of two main modules: the Discrete Wavelet (DW) loss and cross-branch interactions. The DW loss decomposes rendered and ground-truth views into levels of frequencies, and minimizes the differences in their frequency representations. By setting a higher weight for low-frequency differences, we can explicitly prioritize them in earlier training stages, thereby reducing overfitting on high frequencies. This represents a *regularization-based* approach that is frequency-centric. On the other hand, the cross-branch modules utilize multi-head attention to capture interactions not only between colors and densities but also among neighboring 3D points. This helps mitigate overfitting to high-frequency details by constraining color predictions through density-based, position-aware relationships. This also represents a *model-based* method that is compatible with INGP, which is highly sensitive to architectural changes.

### 4.2. Scene Decomposition with Discrete Wavelet loss

Given a pair of predicted view  $\mathbf{I}$  and ground-truth view  $\mathbf{I}_{gt}$ , the Discrete Wavelet (DW) loss minimizes the differences of their frequency representations:

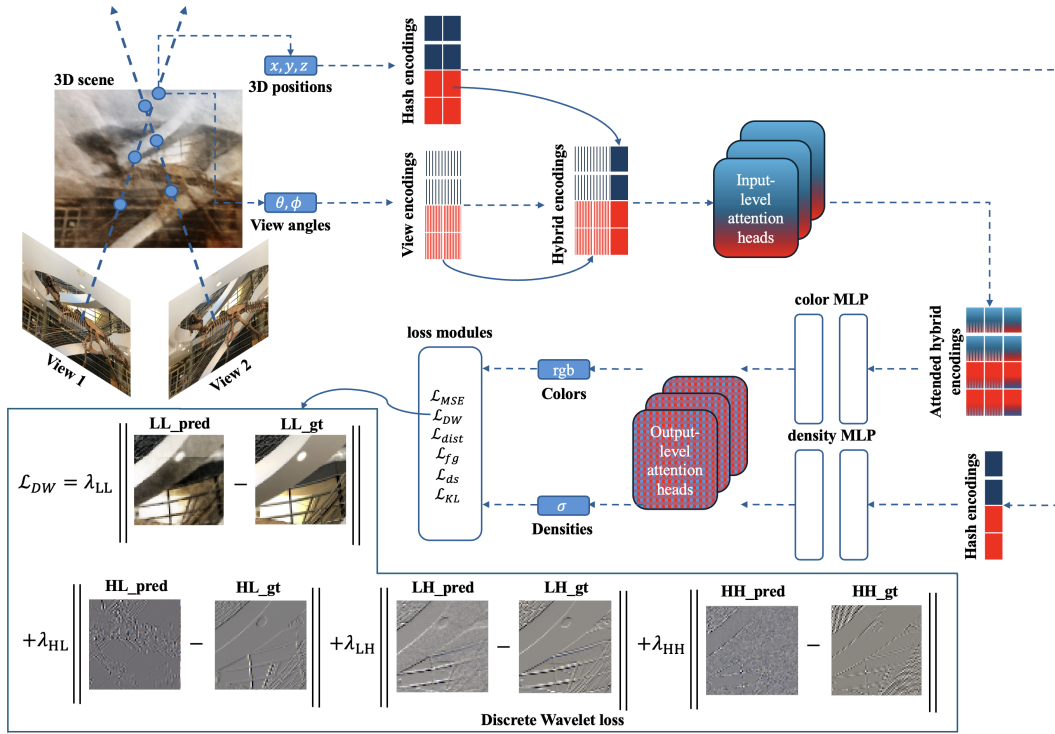


Figure 2. Architecture diagram of DWTNeRF. Firstly, we encode 3D positions with INGP’s [22] hash encoding, and the viewing directions with spherical harmonics [27]. Afterwards, we concatenate the view encodings with the hash encodings, to produce the “hybrid encodings”. We facilitate cross-branch interactions by feeding them into a multi-head attention [34] module. The attended hybrid encodings are inputs to the color MLP, while the hash encodings are inputs to the density MLP. Then, the MLP outputs from both branches are concatenated together, and again fed into another multi-head attention module. To supervise the quality of novel views, we use the usual photometric loss ( $\mathcal{L}_{MSE}$ ) between the predicted and ground-truth views, as well as other regularization terms that are used in CombiNeRF [2].

$$\mathcal{L}_{DW} = \lambda_{LL} \|\mathbf{I}^{LL} - \mathbf{I}_{gt}^{LL}\|_2^2 + \lambda_{LH} \|\mathbf{I}^{LH} - \mathbf{I}_{gt}^{LH}\|_2^2 + \lambda_{HL} \|\mathbf{I}^{HL} - \mathbf{I}_{gt}^{HL}\|_2^2 + \lambda_{HH} \|\mathbf{I}^{HH} - \mathbf{I}_{gt}^{HH}\|_2^2$$

where  $\lambda_{LL}$  is the weighting for the LL sub-band, and so on for other sub-bands. By setting  $\lambda_{LL}$  higher relative to other sub-bands, we have explicitly prioritized learning of low frequencies. The DW loss is incorporated with the photometric loss  $\mathcal{L}_{MSE}$ , as well as all regularization losses used in CombiNeRF [2]:

$$\mathcal{L} = \mathcal{L}_{MSE} + \mathcal{L}_{DW} + \lambda_{dist} \mathcal{L}_{dist} + \lambda_{fg} \mathcal{L}_{fg} + \lambda_{ds} \mathcal{L}_{ds} + \lambda_{KL} \mathcal{L}_{KL}$$

where  $\mathcal{L}_{dist}$  is the distortion loss, introduced by MipNeRF 360 [1].  $\mathcal{L}_{fg}$  is the full geometry loss, introduced by DiffusionNeRF [37].  $\mathcal{L}_{ds}$  is the depth smoothness loss, introduced by RegNeRF [23].  $\mathcal{L}_{KL}$  is the KL divergence loss, introduced by InfoNeRF [16]. The DW loss allows us to prioritize low frequencies directly in the training objective.

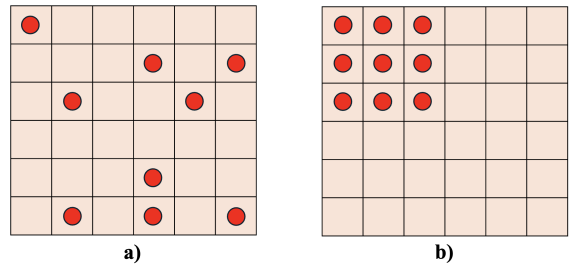


Figure 3. Random (left) and patch-based ray sampling (right). Patch sampling immediately forms a 2D image, and is compatible with the Discrete Wavelet Transform.

**Patch-based Rendering** The DW loss requires adjacently sampled rays  $\mathbf{r}$  that make up a 2D image  $\mathbf{I}$ . This requires patch-based ray sampling. As illustrated in Figure 3b, rays sampled in patches are adjacent to each other, making up a small square grid. Figure 3a shows rays sampled randomly



---

**Algorithm 1** DWTNeRF Training Algorithm

---

**Input:** Dataset of observed views  $\mathcal{D} = \{(\mathbf{I}_{full}, \mathbf{p})\}$ , with pose  $\mathbf{p}$  for each full-resolution image  $\mathbf{I}_{full}$ ; current iteration  $t$ ; maximum iteration  $T$ ; randomly sampled batch size  $|\mathcal{R}|$ ; patch-based sampled batch size  $|\mathcal{R}_P|$ ; DW loss’s interval  $K_{DW}$ ; DW loss’s maximum iteration  $T_{DW}$ ; sub-band weights  $\lambda_{(\cdot)}$ ; learning rate  $\eta_t$

**Output:** Trained NeRF  $f_{\theta}(\cdot, \cdot)$

Initialize NeRF  $f_{\theta}(\cdot, \cdot)$

**repeat**

Randomly sample a ray batch  $\mathcal{R}$ , with corresponding ground-truth colors  $\mathbf{c}_{gt}(\mathcal{R})$

Compute predicted colors  $\mathbf{c}(\mathcal{R})$  by Eq. (1)

$\mathcal{L} \leftarrow \mathcal{L}_{MSE}(\mathbf{c}(\mathcal{R}), \mathbf{c}_{gt}(\mathcal{R}))$

**if**  $t \bmod K_{DW} = 0$  **and**  $t < T_{DW}$  **then**

Sample a patch-based ray batch  $\mathcal{R}_P$ , with corresponding ground-truth colors  $\mathbf{c}_{gt}(\mathcal{R}_P) \equiv \mathbf{I}_{gt}$

Compute predicted colors  $\mathbf{c}(\mathcal{R}_P) \equiv \mathbf{I}$  by Eq. (1)

Compute predicted sub-bands  $\mathbf{I}^{LL}, \mathbf{I}^{LH}, \mathbf{I}^{HL}, \mathbf{I}^{HH}$

Compute ground-truth sub-bands  $\mathbf{I}_{gt}^{LL}, \mathbf{I}_{gt}^{LH}, \mathbf{I}_{gt}^{HL}, \mathbf{I}_{gt}^{HH}$

$\mathcal{L} \leftarrow \mathcal{L} + \mathcal{L}_{DW}(\mathbf{I}^{(\cdot)}, \mathbf{I}_{gt}^{(\cdot)})$

**end if**

$\theta \leftarrow \text{Adam}(\theta, \eta_t, \nabla_{\theta} \mathcal{L})$

**until**  $t > T$

---

throughout the image grid. We use random ray sampling for calculating  $\mathcal{L}_{MSE}$ , and patch-based for  $\mathcal{L}_{DW}$ . This design choice is intentional: it considers both global structures (random rays) and local structures (patch-based rays) in one iteration.

**Lazy Regularization** The sub-bands are 4 times smaller than the original image  $\mathbf{I}$ . For the DW loss to be feasible, however, the sub-bands still need to be visually meaningful. For example,  $\mathbf{I}^{LH}$  and  $\mathbf{I}^{HL}$  can highlight vertical and horizontal edges of a scene. By minimizing their differences with the ground-truths, we can better preserve those mid-frequency-level structures. This requires the rendered image  $\mathbf{I}$  to be large in the first place, or else its sub-bands would be too coarse. This incurs heavy computational overhead, because an  $N$ -sized square patch requires  $N^2$  number of rays. We alleviate the problem as follows. Firstly, we follow the lazy regularization procedure inspired by [14], where we only calculates the DW loss every few iterations. Secondly, since we only prioritize low frequencies earlier in the training, we can safely stop calculating the DW loss later on. We present the full training algorithm of DWTNeRF at Algorithm 1. Here, we only detail  $\mathcal{L}_{MSE}$  and  $\mathcal{L}_{DW}$  for simplicity.

### 4.3. Cross-branch Interactions with Multi-head Attention

Our approach towards cross-branch interactions consists of three stages:

**I. Cross-branch Concatenation** We are given the hash encoding  $\gamma_{0:N_x}(\mathbf{x})$  and the view encoding  $\gamma_{0:N_d}(\mathbf{d})$ . Here, the subscripts denote the dimension of the encoding.  $0 : N_{(\cdot)}$  means the full dimension.  $N_x$  and  $N_d$  represent the highest dimensions of the hash and view encodings. The first stage involves concatenating the view encoding with all-but-the-first-dimension of the hash encoding. This can be written as  $\gamma'(\mathbf{d}, \mathbf{x}) = [\gamma(\mathbf{d}), \gamma_{1:N_x}(\mathbf{x})]$ , where  $[\cdot, \cdot]$  denotes the concatenation operator. We call this the “hybrid encoding”. The hash encoding only retains its first dimension:  $\gamma'(\mathbf{x}) = \gamma_0(\mathbf{x})$ . The intuition is as follows. We will use  $\gamma'(\mathbf{x})$  as inputs to the density MLP, and  $\gamma'(\mathbf{d}, \mathbf{x})$  as inputs to the color MLP. Densities are irrespective of viewing directions and should only be position-dependent, so we make  $\gamma'(\mathbf{x})$  extremely lean to avoid over-parameterizing them. On the other hand, colors are both view- and position-dependent, which explains the concatenation.

**II. Input-level Multi-head Attention** We now have the “trimmed” hash encoding  $\gamma'(\mathbf{x})$  and hybrid encoding  $\gamma'(\mathbf{d}, \mathbf{x})$ . We push  $\gamma'(\mathbf{d}, \mathbf{x})$  into a multi-head attention module to learn the interactions between  $\gamma(\mathbf{d})$  and  $\gamma_{1:N_x}(\mathbf{x})$ . Again, we leave  $\gamma'(\mathbf{x})$  intact to not over-parameterize it. The multi-head attention is applied as:  $\text{MultiHead}(\mathbf{Q}, \mathbf{K}, \mathbf{V}) = [\text{head}_0, \dots, \text{head}_H] \mathbf{W}^O$ , where  $\text{head}_i = \text{Attn}(\mathbf{Q} \mathbf{W}_i^Q, \mathbf{K} \mathbf{W}_i^K, \mathbf{V} \mathbf{W}_i^V)$ . Here,  $\text{Attn}$  is simply the attention layer [34].  $\mathbf{Q}, \mathbf{K}, \mathbf{V}$  are the query, key and value matrices, all of which are set to  $\gamma'(\mathbf{d}, \mathbf{x})$ .  $\mathbf{W}_i^Q, \mathbf{W}_i^K, \mathbf{W}_i^V$  are the corresponding learnable projection matrices. We note that  $\gamma'(\mathbf{d}, \mathbf{x})$  is a tensor of size  $|\mathcal{R}| \times (N_x - 1 + N_d)$ . The choice of using attention is deliberate. Along the vertical dimension, it learns the interactions between all rays  $\mathbf{r}$  in the batch  $\mathcal{R}$ . This equates to learning the interactions between neighboring 3D points. Along the horizontal dimension, it learns the interactions between the positions and viewing directions. Using many heads, up to a maximum  $H$ , provides many of such interactions. The heads are concatenated, and then projected by another learnable matrix  $\mathbf{W}^O$  to ensure outputs and inputs are of the same size. We now write the attended hybrid encoding as  $\gamma''(\mathbf{d}, \mathbf{x})$ . The plenoptic function is now  $f(\gamma'(\mathbf{x}), \gamma''(\mathbf{d}, \mathbf{x})) = \sigma, \mathbf{c}$ , parameterized by two separate MLP branches for densities and colors.

**III. Output-level Multi-head Attention**  $f$ ’s outputs are the “preliminary” colors  $\mathbf{c}$  and densities  $\sigma$ . We again learn their interactions. We concatenate them together, and feed them into a multi-head attention module. Here,  $\mathbf{Q}, \mathbf{K}, \mathbf{V}$  are set to  $\zeta = [\sigma, \mathbf{c}]$ . All intuitions in the second stage still hold. We “un-concatenate” the attended  $\zeta'$  to obtain the final predictions. Specifically, the densities  $\sigma'$  are the first

dimension of  $\zeta'$ , and the colors  $c'$  are the three remaining dimensions.

## 5. Experiments

### 5.1. Datasets & Implementation Details

**Datasets & Metrics** DWTNeRF is evaluated on the LLFF [20] dataset and the NeRF-Synthetic dataset [21], under few-shot conditions. Those are popular benchmarks for novel view synthesis. For the LLFF dataset, we evaluated the test metrics under 2/3/6/9 input views. For the NeRF-Synthetic (NS) dataset, we trained on 4 views and tested on 25 views. Those protocols are similar to previous works. We employed the PSNR, SSIM [35] and LPIPS [43] metrics to evaluate the quality of novel views.

**Implementation Details** Our implementation is built on top of CombiNeRF [2], which in turn is built on a Pytorch re-implementation of INGP, torch-ngp [31]. We refer to torch-ngp as “Vanilla NeRF”. We kept all default settings of CombiNeRF, and trained for 10K iterations in all experiments. We randomly sampled 4096 rays (for LLFF) and 7008 rays (for NS) in each iteration. For the DW loss, we additionally sampled 36864 rays, leading to a  $192 \times 192$  square patch. We calculated the DW loss every 10 (for LLFF) and 150 (for NS) iterations, but stopped altogether at 5K iterations to facilitate high-frequency learning. We used the Haar filter for the DWT. For LLFF, we set the LL sub-band weight as 0.4, the other sub-bands were 0.2. For NS, LL sub-band weight was 0.04, the rest were all 0.02. This ensures that the low frequencies were the most important. Finally, we used 2 (for LLFF) and 1 (for NS) attention heads for both input and output levels. All trainings were done with NVIDIA’s GeForce RTX 4070 Ti Super with 16GB VRAM.

### 5.2. Qualitative Results

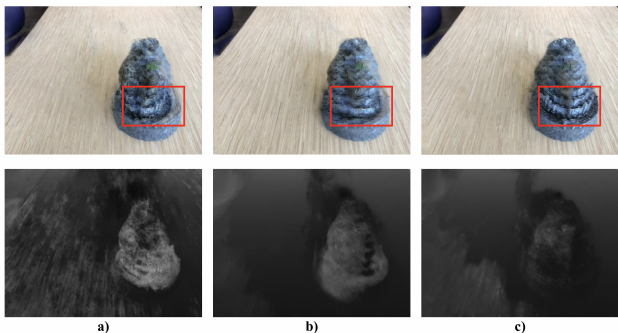


Figure 4. Qualitative results for Vanilla NeRF (a), CombiNeRF (b) and DWTNeRF (c) (“fortress” scene). Our DWTNeRF retains finer details better, as depicted in the red region.

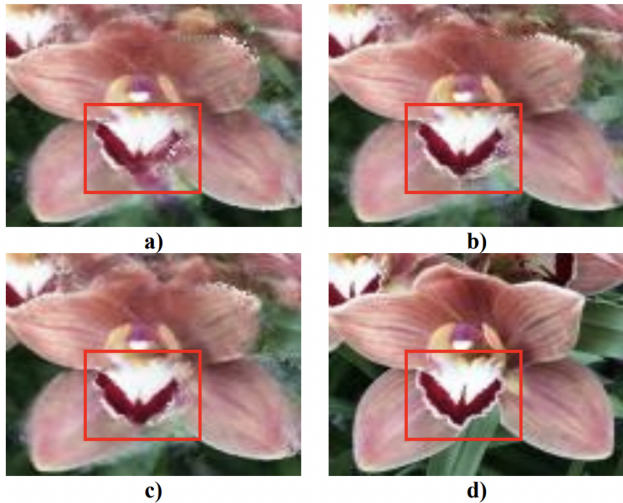


Figure 5. Qualitative results for CombiNeRF (a), DWTNeRF with no DW loss (b), DWTNeRF with both modules (c) and ground-truth (d) (“orchids” scene). Using the DW loss preserves structures better, which in turn produces the least pink-colored “hallucinations”, as depicted in the red region.

Figure 4 shows the qualitative results between Vanilla NeRF, CombiNeRF and our DWTNeRF. The chosen scene is “fortress”. The top row shows the rendered novel views. Our DWTNeRF clearly retains the lower-half structures of the fortress. The bottom row shows the corresponding depth maps. Both CombiNeRF and DWTNeRF dramatically lessen floating artifacts that are extremely prevalent in Vanilla NeRF. DWTNeRF’s depth maps are also more factual than CombiNeRF: the fortress should generally be as far to the camera as the table.

Figure 5 shows a more ablation-level analysis that demonstrates the effects of using the DW loss. The chosen scene is “orchids”. With the DW loss, we additionally gain a supervision on the low- and middle frequencies. This translates to better preserved structures, and less 3D “hallucinations”.

### 5.3. Quantitative Results

**On LLFF** We compared DWTNeRF against recent few-shot works published at top venues. Regularization-based methods include InfoNeRF [16], FreeNeRF [39] and CombiNeRF [2]. Prior-based methods include DietNeRF [11], RegNeRF [23] and GeCoNeRF [17]. Model-based method includes mi-MLP [46]. Table 1 shows the quantitative results. Methods with the symbol † were reproduced on our machine, but all default settings from the corresponding GitHub repository were kept intact. Unavailable metrics are denoted with “–”. The best-performing metrics under each few-shot condition are **bolded**. In the 2-shot case, DWTNeRF outperforms CombiNeRF by 1.6% in PSNR, 0.84%

Table 1. Comparison of DWTNeRF against SOTA methods under 2/3/6/9 views, LLFF dataset [20]

METHOD	VENUE	PSNR (↑)				SSIM (↑)				LPIPS (↓)			
		2-VIEW	3-VIEW	6-VIEW	9-VIEW	2-VIEW	3-VIEW	6-VIEW	9-VIEW	2-VIEW	3-VIEW	6-VIEW	9-VIEW
VANILLA NeRF [31]	ARXIV '22	16.59	17.71	22.03	24.21	0.458	0.544	0.738	0.811	0.359	0.303	0.149	0.101
REGNeRF [23]	CVPR '22	-	19.08	23.10	24.86	-	0.587	0.760	0.820	-	0.336	0.206	0.161
GeCoNeRF [17]	ICML '23	-	18.77	-	-	-	0.596	-	-	-	0.338	-	-
FREENeRF [39]	CVPR '23	-	19.63	23.73	25.13	-	0.612	0.779	0.827	-	0.308	0.195	0.160
MI-MLP [46]	CVPR '24	-	19.75	23.57	25.15	-	0.614	0.788	0.834	-	0.300	0.163	0.140
COMBiNeRF [2] †	3DV '24	16.47	20.12	<b>24.05</b>	<b>25.24</b>	0.475	0.676	<b>0.801</b>	<b>0.836</b>	0.336	0.197	0.105	<b>0.084</b>
DWTNeRF (OURS)	-	<b>16.73</b>	<b>20.38</b>	24.04	25.20	<b>0.479</b>	<b>0.677</b>	<b>0.801</b>	0.835	<b>0.322</b>	<b>0.193</b>	<b>0.104</b>	<b>0.084</b>

Table 2. Comparison of DWTNeRF against SOTA methods under 4 views, NeRF-Synthetic dataset [21]

METHOD	VENUE	PSNR (↑)	SSIM (↑)	LPIPS (↓)
DIETNeRF [11]	ICCV '21	15.42	0.730	0.314
VANILLA NeRF [31] †	ARXIV '22	17.49	0.734	0.357
REGNeRF [23]	CVPR '22	13.71	0.786	0.346
INFONeRF [16]	CVPR '22	18.44	0.792	<b>0.223</b>
COMBiNeRF [2] †	3DV '24	18.72	0.782	0.269
DWTNeRF (OURS)	-	<b>19.06</b>	<b>0.793</b>	0.226

in SSIM and 4.17% in LPIPS. The effects of our DWTNeRF are still strongly seen with 3-shot, but generally fade with higher views, suggesting its high compatibility with extreme few-shot conditions.

**On NeRF-Synthetic** Table 2 shows the quantitative results. In the 4-shot case, DWTNeRF outperforms CombiNeRF by 1.8% in PSNR, 1.4% in SSIM and 15.9% in LPIPS.

### 5.4. Ablation studies

In this section, we examined the contributions of DWTNeRF’s modules. All ablations were done on the LLFF dataset, under 3-shot condition.

**On main modules** Those are the DW loss and the cross-branch interactions. Table 3 shows the effects of each module. The second row removes the frequency masking from CombiNeRF, given its incompatibility with INGP-based models. This provides improvements in all metrics. The third row is our DWTNeRF, but with the DW loss only. Starting from the fourth row, we examine the effects of using multi-head attention in cross-branch interactions. The fourth row is DWTNeRF with only input-level attention. The fifth row only has output-level attention. The sixth row combines both levels. This produces stronger results over the previous two. The final row combines both DW loss and cross-branch interactions, which provides the strongest results.

**On prior-based methods** We implemented two prior-based approaches on top of CombiNeRF: DietNeRF’s semantic consistency (SC) loss [11] and SPARF’s multi-view (MV) correspondence loss [33]. We simply replaced the DW loss at Algorithm 1 with these losses. Table 4 (upper half)

Table 3. Ablation on DWTNeRF’s main modules, LLFF dataset [20]

METHOD	PSNR (↑)	SSIM (↑)	LPIPS (↓)
COMBiNeRF [2] (BASELINE) †	20.12	0.676	0.197
COMBiNeRF [2] (-FREQ. MASK.) †	20.19	<b>0.677</b>	0.194
DWTNeRF (+DW.)	20.25	<b>0.677</b>	<b>0.193</b>
DWTNeRF (+INP. ATTN.)	20.33	0.670	0.195
DWTNeRF (+OUTP. ATTN.)	20.34	0.670	0.195
DWTNeRF (+FULL CB.)	20.36	0.670	0.195
DWTNeRF (+BOTH)	<b>20.38</b>	<b>0.677</b>	<b>0.193</b>

Table 4. Comparison against prior-based and model-based methods, LLFF dataset [20]

METHOD	TYPE	PSNR (↑)	SSIM (↑)	LPIPS (↓)
COMBiNeRF [2] (BASELINE) †	R	20.12	0.676	0.197
DIETNeRF [11] (+FULL CB.) †	M, P	20.36	<b>0.677</b>	<b>0.192</b>
SPARF [33] (+FULL CB.) †	M, P	19.28	0.618	0.261
DWTNeRF (+FULL CB. + DW.)	M, R	<b>20.38</b>	<b>0.677</b>	0.193
COMBiNeRF [2] (BASELINE) †	R	20.12	<b>0.676</b>	0.197
COMBiNeRF [2] (+RES.) †	M, R	20.20	0.664	0.198
COMBiNeRF [2] (+RES.+) †	M, R	19.99	0.650	0.204
COMBiNeRF [2] (+ELE. CB.) †	M, R	19.90	0.667	0.205
DWTNeRF (+FULL CB.)	M, R	<b>20.36</b>	0.670	<b>0.195</b>

shows the results. “R”, “P”, “M” stand for regularization-, prior- and model-based, respectively. Our DW loss is competitive with SC loss, but the DWT is much more lightweight than computing feature embeddings from a CLIP model. This suggests frequency supervision can be as important as semantic supervision. Performance worsens with MV loss, suggesting the multi-view correspondences are not a useful prior for INGP.

**On model-based methods** We implemented two model-based approaches on top of CombiNeRF: “Residual Connections” and “Element-wise Cross-branch Interactions” - both introduced by mi-MLP [46]. Table 4 (lower half) shows the results. The second row shows “Residual Connections” built on top of CombiNeRF. The third row is the same, but we added one MLP layer to both the density & color branches, hoping this could better highlight the effects of using “Residual Connections”. However, increasing layers degraded per-



Table 5. Low-pass filters of the Daubechies wavelets

ORDER	1	2	3
$l_k$	1	$1 + \sqrt{3}$	0.3327
	1	$3 + \sqrt{3}$	0.8069
		$3 - \sqrt{3}$	0.4599
		$1 - \sqrt{3}$	-0.1350
			-0.0854
			0.0352
FACTOR	$\sqrt{2}$	$4\sqrt{2}$	1

Table 6. Ablation on wavelets for DW loss

METHOD	PSNR ( $\uparrow$ )	SSIM ( $\uparrow$ )	LPIPS ( $\downarrow$ )
COMBINeRF [2] (BASELINE) $\dagger$	20.12	0.676	0.197
DWTNeRF (+DW. / HAAR)	<b>20.25</b>	0.677	0.193
DWTNeRF (+DW. / DB2)	20.23	<b>0.678</b>	0.193
DWTNeRF (+DW. / DB3)	20.23	<b>0.678</b>	<b>0.192</b>

formances noticeably, highlighting the vulnerability of INGP to architectural changes. The fourth row shows “Element-wise Cross-branch Interactions”. Only our cross-branch interaction method is competitive with baseline.

**On the choice of wavelets** We compared the effects of different Daubechies wavelets [6] on the DW loss. We started with the Haar ( $n = 1$ ) and then higher-order wavelets, up to the db3 ( $n = 3$ ). The wavelet coefficients are shown in Table 5. Generally, higher-order wavelets have more supports, and spreads the signal energy more evenly across sub-bands. Figure 6 compares scene decomposition using the Haar versus db2 ( $n = 2$ ). Compared to the ground-truth sub-bands, the rendered sub-bands are much noisier, highlighting the purpose of the DW loss. The db2 provides finer details. However, table 6 shows no significant differences between the wavelets. This confirms our intuition that low-frequency supervision is sufficient. While the db3 is technically the best-performing, it costs more computation due to having more coefficients. Therefore, the Haar became our method of choice.

## 6. Conclusion

INGP-based models have distinct characteristics that might make them incompatible with recent few-shot approaches. Firstly, they are fast-converging, and vulnerable to architectural changes under few-shot conditions. This requires a re-thinking in *model-based* approaches. For this, we introduce a cross-branch interaction pipeline based on multi-head attention, which acts on NeRF’s inputs & outputs, but not on the MLP layers. Secondly, based on multi-resolution, INGP does not explicitly map the inputs into a range of

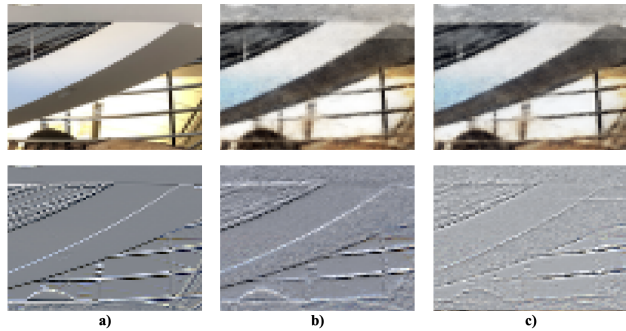


Figure 6. Decomposition using the Haar (a & b) and db2 (c). We only show the LL (top) and LH (bottom) sub-bands. Column a) is the ground-truth LL, much less noisier than rendered LL at column b). Column c) uses higher-order wavelet, and shows finer details.

frequencies. This requires a re-thinking in *frequency- and regularization-based* approaches. For this, we introduce a novel Discrete Wavelet loss that decomposes the scenes into different frequencies and allows explicit prioritization of low frequencies in earlier training stages.

**Limitations & Future Works** Firstly, the DWT does not disentangle high-frequency components. For example, besides fine structural details, high frequencies can come from specularly and other light-dependent effects. Future works might explore scene decomposition at such further levels. Secondly, since the DW loss is used as an auxiliary loss alongside the photometric MSE loss, which compares pixel-wise differences regardless of frequencies, we believe some high-frequency overfitting still exists. Our DW loss *prioritizes* low frequencies, but not *eliminate* high frequencies in early training. Future works could tackle this problem, but interfering with the photometric loss can be tricky. We can also investigate the applicability of our methods to other representations, like SDF [3, 18] or 3DGS [15].

## References

- [1] Jonathan T. Barron, Ben Mildenhall, Dor Verbin, Pratul P. Srinivasan, and Peter Hedman. Mip-nerf 360: Unbounded anti-aliased neural radiance fields. In *2022 IEEE/CVF Conference on Computer Vision and Pattern Recognition (CVPR)*, pages 5460–5469, 2022. 2, 4
- [2] Matteo Bonotto, Luigi Sarrocco, Daniele Evangelista, Marco Imperoli, and Alberto Pretto. CombiNeRF: A Combination of Regularization Techniques for Few-Shot Neural Radiance Field View Synthesis. In *International Conference on 3D Vision (3DV)*, 2024. 2, 4, 6, 7, 8
- [3] T. Chan and Wei Zhu. Level set based shape prior segmentation. In *2005 IEEE Computer Society Conference on Computer Vision and Pattern Recognition (CVPR’05)*, pages 1164–1170 vol. 2, 2005. 8
- [4] Zixuan Chen, Lingxiao Yang, Jian-Huang Lai, and Xiao-



- hua Xie. Cunerf: Cube-based neural radiance field for zero-shot medical image arbitrary-scale super resolution. In *2023 IEEE/CVF International Conference on Computer Vision (ICCV)*, pages 21128–21138, 2023. 1
- [5] Abril Corona-Figueroa, Jonathan Frawley, Sam Bond Taylor, Sarath Bethapudi, Hubert P. H. Shum, and Chris G. Willcocks. Mednerf: Medical neural radiance fields for reconstructing 3d-aware ct-projections from a single x-ray. In *2022 44th Annual International Conference of the IEEE Engineering in Medicine & Biology Society (EMBC)*, pages 3843–3848, 2022. 1
- [6] Ingrid Daubechies. *Ten Lectures on Wavelets*. Society for Industrial and Applied Mathematics, 1992. 8
- [7] Kyle Gao, Yina Gao, Hongjie He, Dening Lu, Linlin Xu, and Jonathan Li. Nerf: Neural radiance field in 3d vision, a comprehensive review, 2023. 2
- [8] Guangcong, Zhaoxi Chen, Chen Change Loy, and Ziwei Liu. Sparsenerf: Distilling depth ranking for few-shot novel view synthesis. *IEEE/CVF International Conference on Computer Vision (ICCV)*, 2023. 2
- [9] Kaiming He, Xiangyu Zhang, Shaoqing Ren, and Jian Sun. Deep residual learning for image recognition. In *2016 IEEE Conference on Computer Vision and Pattern Recognition (CVPR)*, pages 770–778, 2016. 2
- [10] Gao Huang, Zhuang Liu, Laurens Van Der Maaten, and Kilian Q. Weinberger. Densely connected convolutional networks. In *2017 IEEE Conference on Computer Vision and Pattern Recognition (CVPR)*, pages 2261–2269, 2017. 2
- [11] Ajay Jain, Matthew Tancik, and Pieter Abbeel. Putting nerf on a diet: Semantically consistent few-shot view synthesis. In *Proceedings of the IEEE/CVF International Conference on Computer Vision (ICCV)*, pages 5885–5894, 2021. 2, 6, 7
- [12] Kyungmin Jo, Gyumin Shim, Sanghun Jung, Soyoung Yang, and Jaegul Choo. Cg-nerf: Conditional generative neural radiance fields for 3d-aware image synthesis. In *2023 IEEE/CVF Winter Conference on Applications of Computer Vision (WACV)*, pages 724–733, 2023. 2
- [13] James T. Kajiya and Brian Von Herzen. Ray tracing volume densities. *Proceedings of the 11th annual conference on Computer graphics and interactive techniques*, 1984. 3
- [14] Tero Karras, Samuli Laine, Miika Aittala, Janne Hellsten, Jaakko Lehtinen, and Timo Aila. Analyzing and improving the image quality of stylegan. In *2020 IEEE/CVF Conference on Computer Vision and Pattern Recognition (CVPR)*, pages 8107–8116, 2020. 5
- [15] Bernhard Kerbl, Georgios Kopanas, Thomas Leimkühler, and George Drettakis. 3d gaussian splatting for real-time radiance field rendering. *ACM Transactions on Graphics*, 42(4), 2023. 8
- [16] Mijeong Kim, Seonguk Seo, and Bohyung Han. Infonerf: Ray entropy minimization for few-shot neural volume rendering. In *2022 IEEE/CVF Conference on Computer Vision and Pattern Recognition (CVPR)*, pages 12902–12911, 2022. 2, 4, 6, 7
- [17] Minseop Kwak, Jiuhn Song, and Seungryong Kim. Geconerf: Few-shot neural radiance fields via geometric consistency. *arXiv preprint arXiv:2301.10941*, 2023. 2, 6, 7
- [18] Runfa Blark Li, Keito Suzuki, Bang Du, Ki Myung Brian Le, Nikolay Atanasov, and Truong Nguyen. Splatsdf: Boosting neural implicit sdf via gaussian splatting fusion, 2024. 8
- [19] Carl Lindström, Georg Hess, Adam Lilja, Maryam Fatemi, Lars Hammarstrand, Christoffer Petersson, and Lennart Svensson. Are nerfs ready for autonomous driving? towards closing the real-to-simulation gap. In *2024 IEEE/CVF Conference on Computer Vision and Pattern Recognition Workshops (CVPRW)*, pages 4461–4471, 2024. 1
- [20] Ben Mildenhall, Pratul P. Srinivasan, Rodrigo Ortiz-Cayon, Nima Khademi Kalantari, Ravi Ramamoorthi, Ren Ng, and Abhishek Kar. Local light field fusion: Practical view synthesis with prescriptive sampling guidelines. *ACM Transactions on Graphics (TOG)*, 2019. 6, 7
- [21] Ben Mildenhall, Pratul P. Srinivasan, Matthew Tancik, Jonathan T. Barron, Ravi Ramamoorthi, and Ren Ng. Nerf: Representing scenes as neural radiance fields for view synthesis. In *ECCV*, 2020. 1, 2, 6, 7
- [22] Thomas Müller, Alex Evans, Christoph Schied, and Alexander Keller. Instant neural graphics primitives with a multiresolution hash encoding. *ACM Trans. Graph.*, 41(4):102:1–102:15, 2022. 1, 2, 4
- [23] Michael Niemeyer, Jonathan T. Barron, Ben Mildenhall, Mehdi S. M. Sajjadi, Andreas Geiger, and Noha Radwan. Regnerf: Regularizing neural radiance fields for view synthesis from sparse inputs. In *2022 IEEE/CVF Conference on Computer Vision and Pattern Recognition (CVPR)*, pages 5470–5480, 2022. 2, 4, 6, 7
- [24] Matt Pharr, Wenzel Jakob, and Greg Humphreys. *Physically Based Rendering: From Theory to Implementation*. Morgan Kaufmann Publishers Inc., San Francisco, CA, USA, 3rd edition, 2016. 3
- [25] Albert Pumarola, Enric Corona, Gerard Pons-Moll, and Francesc Moreno-Noguer. D-NeRF: Neural Radiance Fields for Dynamic Scenes. In *Proceedings of the IEEE/CVF Conference on Computer Vision and Pattern Recognition*, 2020. 2
- [26] Nasim Rahaman, Aristide Baratin, Devansh Arpit, Felix Draxler, Min Lin, Fred A. Hamprecht, Yoshua Bengio, and Aaron C. Courville. On the spectral bias of neural networks. In *ICML*, pages 5301–5310. PMLR, 2019. 1
- [27] Ravi Ramamoorthi. Modeling illumination variation with spherical harmonics. 2005. 4
- [28] Sara Fridovich-Keil and Alex Yu, Matthew Tancik, Qinhong Chen, Benjamin Recht, and Angjoo Kanazawa. Plenoxels: Radiance fields without neural networks. In *CVPR*, 2022. 1
- [29] Seunghyeon Seo, Yeonjin Chang, and Nojun Kwak. Flipnerf: Flipped reflection rays for few-shot novel view synthesis. In *2023 IEEE/CVF International Conference on Computer Vision (ICCV)*, pages 22826–22836, 2023. 1
- [30] Gilbert Strang and Truong Nguyen. *Wavelets and filter banks*. SIAM, 1996. 3
- [31] Jiayang Tang. Torch-ngp: a pytorch implementation of instant-ngp, 2022. <https://github.com/ashawkey/torch-ngp>. 6, 7
- [32] Adam Tonderski, Carl Lindström, Georg Hess, William Ljungbergh, Lennart Svensson, and Christoffer Petersson.

- Neurad: Neural rendering for autonomous driving. In *Proceedings of the IEEE/CVF Conference on Computer Vision and Pattern Recognition*, pages 14895–14904, 2024. 1
- [33] Prune Truong, Marie-Julie Rakotosaona, Fabian Manhardt, and Federico Tombari. Sparf: Neural radiance fields from sparse and noisy poses. *IEEE/CVF Conference on Computer Vision and Pattern Recognition, CVPR*, 2023. 2, 7
- [34] Ashish Vaswani, Noam Shazeer, Niki Parmar, Jakob Uszkoreit, Llion Jones, Aidan N Gomez, Łukasz Kaiser, and Illia Polosukhin. Attention is all you need. In *Advances in neural information processing systems*, pages 5998–6008, 2017. 4, 5
- [35] Zhou Wang, A.C. Bovik, H.R. Sheikh, and E.P. Simoncelli. Image quality assessment: from error visibility to structural similarity. *IEEE Transactions on Image Processing*, 13(4): 600–612, 2004. 6
- [36] Chung-Yi Weng, Brian Curless, Pratul P. Srinivasan, Jonathan T. Barron, and Ira Kemelmacher-Shlizerman. HumanNeRF: Free-viewpoint rendering of moving people from monocular video. In *Proceedings of the IEEE/CVF Conference on Computer Vision and Pattern Recognition (CVPR)*, pages 16210–16220, 2022. 1
- [37] Jamie Wynn and Daniyar Turmukhambetov. Diffusionerf: Regularizing neural radiance fields with denoising diffusion models. In *2023 IEEE/CVF Conference on Computer Vision and Pattern Recognition (CVPR)*, pages 4180–4189, 2023. 2, 4
- [38] Linning Xu, Vasu Agrawal, William Laney, Tony Garcia, Aayush Bansal, Changil Kim, Samuel Rota Bulò, Lorenzo Porzi, Peter Kotschieder, Aljaž Božič, Dahua Lin, Michael Zollhöfer, and Christian Richardt. VR-NeRF: High-fidelity virtualized walkable spaces. In *SIGGRAPH Asia Conference Proceedings*, 2023. 1
- [39] Jiawei Yang, Marco Pavone, and Yue Wang. Freenerf: Improving few-shot neural rendering with free frequency regularization. In *Proc. IEEE Conf. on Computer Vision and Pattern Recognition (CVPR)*, 2023. 1, 2, 6, 7
- [40] Jianglong Ye, Naiyan Wang, and Xiaolong Wang. Featurenerf: Learning generalizable nerfs by distilling foundation models. In *Proceedings of the IEEE/CVF International Conference on Computer Vision*, pages 8962–8973, 2023. 2
- [41] Alex Yu, Ruilong Li, Matthew Tancik, Hao Li, Ren Ng, and Angjoo Kanazawa. PlenOctrees for real-time rendering of neural radiance fields. In *ICCV*, 2021. 2
- [42] Alex Yu, Vickie Ye, Matthew Tancik, and Angjoo Kanazawa. pixelNeRF: Neural radiance fields from one or few images. In *CVPR*, 2021. 2
- [43] Richard Zhang, Phillip Isola, Alexei A Efros, Eli Shechtman, and Oliver Wang. The unreasonable effectiveness of deep features as a perceptual metric. In *CVPR*, 2018. 6
- [44] Allan Zhou, Moo Jin Kim, Lirui Wang, Pete Florence, and Chelsea Finn. Nerf in the palm of your hand: Corrective augmentation for robotics via novel-view synthesis. In *2023 IEEE/CVF Conference on Computer Vision and Pattern Recognition (CVPR)*, pages 17907–17917, 2023. 1
- [45] Haidong Zhu, Yuyin Sun, Chi Liu, Lu Xia, Jijia Luo, Nan Qiao, Ram Nevatia, and Cheng-Hao Kuo. Multimodal neural radiance field. In *2023 IEEE International Conference on Robotics and Automation (ICRA)*, pages 9393–9399, 2023. 1
- [46] Hanxin Zhu, Tianyu He, Xin Li, Bingchen Li, and Zhibo Chen. Is vanilla mlp in neural radiance field enough for few-shot view synthesis? In *Proceedings of the IEEE/CVF Conference on Computer Vision and Pattern Recognition (CVPR)*, pages 20288–20298, 2024. 1, 2, 6, 7